Inorganic Chemistry

Article

pubs.acs.org/IC

Large Thermal Hysteresis for Iron(II) Spin Crossover Complexes with *N*-(Pyrid-4-yl)isonicotinamide

Charles Lochenie,[†,‡] Wolfgang Bauer,[†] Antoine P. Railliet,[‡] Stephan Schlamp,[†] Yann Garcia,*[,‡] and Birgit Weber*[,†]

[†]Inorganic Chemistry II, Universität Bayreuth, Universitätsstrasse 30, NW I, 95440 Bayreuth, Germany

[‡]Insitute of Condensed Matter and Nanosciences, Molecules, Solids and Reactivity (IMCN/MOST), Université Catholique de Louvain, Place Louis Pasteur 1, 1348 Louvain-la-Neuve, Belgium

Supporting Information

ABSTRACT: A new series of iron(II) 1D coordination polymers with the general formula [FeL1(pina)]·*x*solvent with L1 being a tetradentate $N_2O_2^{2-}$ coordinating Schiff-base-like ligand [([3,3′]-[1,2-phenylenebis-(iminomethylidyne)]bis(2,4-pentanedionato)(2-)-*N*,*N*′,O^2,$O^{2'}$], and pina being a bridging axial ligand *N*-(pyrid-4-yl)isonicotinamide, are discussed. The X-ray crystal structure of [FeL1(pina)]·2MeOH was solved for the low-spin state. The compound crystallizes in the monoclinic space group $P2_1/c$, and the analysis of the crystal packing reveals the formation of a hydrogen bond network where additional methanol molecules are included. Different magnetic properties are observed for the seven samples analyzed, depending on the nature of the included solvent molecules. The widest hysteresis loop is observed for a fine crystalline sample of composition [FeL1(pina)]·*x*H_2O/MeOH. The 88 K wide thermal hysteresis loop ($T_{1/2\uparrow}$ = 328 K and $T_{1/2\downarrow}$ = 240 K) is centered around room temperature and can be repeated without of a loss of the spin transition properties. For the single crystals of [FeL1(pina)]·2MeOH, a 51 K wide hysteresis loop is observed ($T_{1/2\uparrow}$ = 296 K and $T_{1/2\downarrow}$ = 245 K) that is also stable for several cycles. For a powder sample of [FeL1(pina)]·0.5H_2O·0.5MeOH a cooperative spin transition with a 46 K wide hysteresis loop around room temperature is observed ($T_{1/2\uparrow}$ = 321 K and $T_{1/2\downarrow}$ = 275 K). This compound was further investigated using Mössbauer spectroscopy and DSC. Both methods reveal that, in the cooling mode, the spin transition is accompanied by a phase transition while in the heating mode a loss of the included methanol is observed that leads to a loss of the spin transition properties. These results show that the pina ligand was used successfully in a crystal-engineering-like approach to generate 1D coordination polymers and improve their spin crossover properties.

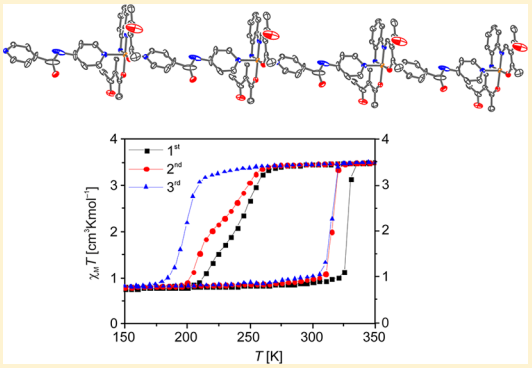

INTRODUCTION

Iron(II) spin crossover (SCO) complexes belong to a fascinating class of materials that can be switched between the paramagnetic high-spin state (HS, S = 2) and the diamagnetic low-spin state (LS, S = 0) by physical stimuli such as temperature, pressure, or light.[1−17] This transition causes electronic, structural, vibrational, and magnetic changes that can be monitored by many different physical methods such as a ^{57}Fe Mössbauer spectroscopy or detected visually due to a color change associated with thermochromism, in many cases. Since their discovery in 1931 by Cambi et al.,[18,19] SCO complexes never cease to attract interest due to the numerous potential applications as memory devices, displays,[20−22] or sensors.[23] The possibility to form micro- and nanoparticles,[24−26] gels[27] or liquid-crystalline materials,[28] reinforced the interest in SCO materials.[29−31] Of the different types of spin transitions (gradual, stepwise, incomplete),[3] SCO complexes exhibiting thermal hysteresis are particularly suited for the mentioned applications. Up to now, the largest hysteresis is a 70 K wide loop for a complex with a Schiff-base-like ligand and imidazole as ligands.[32] It was demonstrated that the crystal packing, especially hydrogen bond network,[33,34] but also structural changes upon spin transition,[35] have a huge influence on the SCO properties of these complexes. We seek to systematically improve the SCO properties of our complexes thanks to crystal engineering to obtain wide and stable hysteresis loops around room temperature. One strategy was to modify the equatorial Schiff-base-like ligand through the introduction of additional hydroxyl groups in the outer periphery to optimize the preconditions for the observation of hydrogen bond networks. This strategy was not successful for mononuclear complexes with pyridine or 4-dimethylaminopyridine as axial ligand.[36] However, for the corresponding 1D coordination polymers with bridging axial ligands as 4,4′-bipyridine or bis(4-pyridyl)ethene, an increased occurrence of thermal hysteresis loops was observed.[37]

Received: July 8, 2014
Published: October 14, 2014

   dx.doi.org/10.1021/ic501624b | *Inorg. Chem.* 2014, 53, 11563−11572

Scheme 1. General Structure of the Ligands and Complexes: Abbreviations Used and Synthesis Pathway of the [FeL1(pina)] Complexes

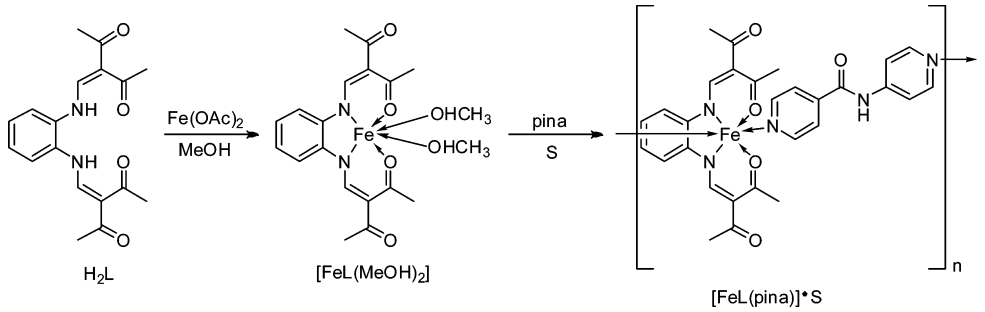

In this work we present an alternative approach to improve the hydrogen network between the polymer chains of Schiff-base-like iron(II) SCO complexes. The objective was to build the hydrogen bond network through the crystal packing by using the pina ligand, which itself is known to make a hydrogel.[38] For this, iron(II) complexes made of a Schiff-base-like equatorial ligand and a bridging *N*-(pyrid-4-yl)-isonicotinamide (pina) axial ligand were synthesized. It has recently been shown that the solvent or the method of synthesis can have a crucial influence on SCO complexes of this ligand family[39a] and of other SCO systems.[39b,c] Therefore, complex [FeL1(pina)] (**1**) was synthesized in various solvents using three different methods. Seven phases that vary in the amount of solvent included in the crystal packing were obtained. All samples were investigated by SQUID magnetometry, the most interesting samples being investigated further using Mössbauer spectrometry, DSC measurements, and single crystal X-ray diffraction, when appropriate.

EXPERIMENTAL SECTION

Synthesis. All reagents were of reagent grade and used without further purification. MeOH and EtOH were purified by distillation under argon,[40] DMF was dried on molecular sieves and degassed, and THF and water were degassed. All syntheses were carried out under argon using Schlenk tube techniques. IR spectra were recorded on a Shimadzu FTIR-84005 spectrometer using KBr discs at room temperature. CHN analyses were performed at MEDAC Ltd. (U.K.). Mass spectra were recorded with a Jeol MS-700 device, with DEI+ as ionization method.

The synthesis is performed in two steps starting from iron(II) acetate and a Schiff-base-like ligand H_2L1 that are reacted to give a first complex [FeL1(MeOH)$_2$] that is then converted with pina in the solvent S to give [FeL1(pina)]·*x*S (Scheme 1). The syntheses of the ligand H_2L1,[41] the pina ligand,[38] iron acetate,[42] and the complex [FeL1(MeOH)$_2$][43] have been performed as previously described. All syntheses except that of **1**·*x*MeOH/H_2O were reproduced at least once.

*[FeL1(pina)]·0.5 MeOH (**1**·0.5 MeOH).* A solution of [FeL1(MeOH)$_2$] (0.55 g) and pina (1.08 g) in methanol (45 mL) was heated to reflux for 1 h. The formation of a dark violet precipitate was observed in the boiling heat. After cooling and filtration, the precipitate was washed with methanol (2 × 5 mL) and dried *in vacuo*. Yield: 0.51 g, 74%. IR (KBr): $\tilde{\upsilon}$ = 3229(w) (NH), 1687(m) (CO), 1647(s) (CO), 1560(vs) cm^{-1} (CO). MS (DEI-(+), 70 eV) *m*/*z* (%): 382 (70) [FeL1+], 199 (97) [pina+], 106 (100). Elemental analysis calcd (found) for $C_{29.5}H_{29}FeN_5O_{5.5}$ (597.15): C 59.3 (59.3), H 4.7 (4.9), N 11.4 (11.7).

*[FeL1(pina)]·xMeOH/H_2O (**1**·xMeOH/H_2O).* Amorphous black crystals of the composition **1**·*x*MeOH/H_2O were obtained by slow diffusion using a homemade Schlenk of [FeL1(MeOH)$_2$] (0.11 g, 0.25 mmol) and pina (0.24 g, later analysis revealed that there were still traces of water in the ligand, for all further approaches the ligand was dried completely) in methanol solution after 2 weeks. Elemental analysis calcd (found) for $C_{29}H_{27}FeN_5O_5$ (581.40, since the exact solvent composition is unknown, the calculated values correspond to the solvent-free complex): C 59.91 (58.5), H 4.68 (4.9), N 12.05 (11.7).

*[FeL1(pina)]·2MeOH (**1**·2MeOH).* Violet crystals of sufficient quality for X-ray analysis were obtained by slow diffusion techniques of [FeL1(MeOH)$_2$] (0.12 g) and pina (0.27 g) in methanol solution after 1 week. Elemental analysis calcd (found) for $C_{31}H_{35}FeN_5O_7$ (645.49): C 57.7 (57.4), H 5.5 (5.0), N 10.9 (10.8).

*[FeL1(pina)]·0.5 H_2O·0.5 MeOH (**1**·0.5H_2O·0.5MeOH).* [FeL1(MeOH)$_2$] (0.5 g) was dissolved in 20 mL mixture of methanol and water (98:2). Pina (0.22 g) was dissolved in 20 mL of the same mixture. Then the pina solution was added to the [FeL1(MeOH)$_2$] solution, and the mixture was stirred 2 h at room temperature. A dark purple powder precipitated, and was filtered, washed twice with 5 mL of MeOH, and carefully dried *in vacuo*. Yield: 0.6 g, 95%. IR (KBr): $\tilde{\upsilon}$ = 3165(b) (OH), 1685(m) (CO), 1593(s) (CO), 1555(vs) cm^{-1} (CO). TGA on 5.7470 mg at 25 °C: 5.5513 mg at 100 °C (−3.405% -solvent loss, theory −4.12%), 3.8603 mg at 315 °C (−32.835% −decomposition). Elemental analysis calcd (found) for $C_{29.5}H_{30}FeN_5O_6$ (606.43): C 58.43 (58.4), H 4.99 (4.9), N 11.55 (11.6).

*[FeL1(pina)]·0.5 EtOH (**1**·0.5 EtOH).* A solution of [FeL1(MeOH)$_2$] (0.41 g) and pina (1.85 g) in ethanol (20 mL) was refluxed for 1 h. A dark red powder precipitated, and was filtered, washed twice with 5 mL of EtOH, and carefully dried *in vacuo*. Yield: 0.49 g, 87%. IR (KBr): $\tilde{\upsilon}$ = 3234(w) (NH), 1678(m) (CO), 1658(s) (CO), 1574(vs) cm^{-1} (CO). MS (DEI-(+), 70 eV) *m*/*z* (%): 382 (70) [FeL1+], 199 (97) [pina+], 106 (100). Elemental analysis calcd (found) for $C_{30}H_{30}FeN_5O_{5.5}$ (604.44): C 59.6 (59.3), H 5.0 (4.9), N 11.6 (11.7).

*[FeL1(pina)]·DMF (**1**·DMF).* A solution of [FeL1(MeOH)$_2$] (0.69 g) and pina (3.1 g) in DMF (20 mL) was refluxed for 1 h. Dark purple crystals appeared after one night at room temperature, and were filtered, washed twice with 5 mL of DMF, and carefully dried *in vacuo*. Yield: 0.51 g, 52%. IR (KBr): $\tilde{\upsilon}$ = 3221(w) (NH), 1675(m) (CO), 1646(s) (CO), 1559(vs) cm^{-1} (CO). MS (DEI-(+), 70 eV) *m*/*z* (%): 382 (70) [FeL1+], 199 (97) [pina+], 106 (100). TGA on 25.31 mg at 25 °C; 24.75 mg at 200 °C (−3.2% −solvent loss), 13.14 mg at 315 °C (−39.9% −decomposition). Elemental analysis calcd (found) for $C_{32}H_{34}FeN_6O_6$ (654.49): C 58.7 (58.6), H 5.2 (5.3), N 12.8 (12.8).

*[FeL1(pina)]·2 H_2O (**1**·2H_2O).* [FeL1(MeOH)$_2$] (0.62 g) was dissolved in 40 mL of THF. Pina (2.7 g) was dissolved in 40 mL of THF. Then, the pina solution was added to the [FeL1(MeOH)$_2$] solution, and the mixture was stirred overnight at room temperature. A red powder precipitated, and was filtered, washed twice with 5 mL of THF, and carefully dried *in vacuo*. Yield: 0.85 g, quantitative. IR (KBr): $\tilde{\upsilon}$ = 3205(w) (NH−OH), 1689(m) (CO), 1653(s) (CO), 1547(vs) cm^{-1} (CO). MS (DEI-(+), 70 eV) *m*/*z* (%): 382 (70) [FeL1+], 199 (97) [pina+], 106 (100). Elemental analysis calcd (found) for $C_{29}H_{31}FeN_5O_7$ (617.16): C 56.2 (56.24), H 5.0 (4.9), N 11.3 (10.9).

X-ray Structure Analysis. The intensity data of **1**·2MeOH were collected on an Oxford XCalibur diffractometer by using graphite-monochromated Mo Kα radiation. The data were corrected for

dx.doi.org/10.1021/ic501624b | *Inorg. Chem.* 2014, 53, 11563−11572

Table 1. Overview of the SCO Behavior, Characteristic $\chi_M T$ Values [cm^3 K mol^{-1}], HS Residue (γ_{HS}) at 150 K, and $T_{1/2}$ Values [K]

compound	spin state behavior	$\chi_M T$ (350 K)	$\chi_M T$ (150 K)	γ_{HS} (150 K)	$T_{1/2}$
1·0.5MeOH	HS	3.33	3.24		
1·*x*MeOH/H_2O	hysteresis, 88 K,[a] 92 K[b]	3.49	0.76	0.2	↓240, ↑328[a] ↓224, ↑316[b]
1·2MeOH	complete, hysteresis, 34 K,[a] 51 K,[b] 45 K[c]	3.64	0.2	0	↓272, ↑306[a] ↓245, ↑296[b] ↓236, ↑281[c]
1·0.5H_2O·0.5MeOH	incomplete, unstable, hysteresis, 46 K,[a] 65 K,[b] 73 K[c]	3.23	1.41,[a] 2.07,[b] 2.29[c]	0.40,[a] 0.59,[b] 0.65[c]	↓275, ↑321[a] ↓263, ↑328[b] ↓238, ↑311[c]
1·0.5EtOH	HS	3.53	3.46		
1·2H_2O	HS	3.44			
1·DMF	solvent release, hysteresis, 4 K,[b] 10 K[c]	3.42	0.08,[a] 0.64,[b] 1.08[c]	0,[a] 0.19,[b] 0.30[c]	↑335[a,d] ↓305, ↑309[b] ↓288, ↑298[c]

[a]Magnetic measurement: loop 1. [b]Loop 2. [c]Loop 3. [d]Spin transition upon solvent release. The exact temperature depends on the scan rate.

Lorentz and polarization effects. The structure was solved by direct methods (SIR-97)[44] and refined by full-matrix least-squares techniques against $F_o^2 - F_c^2$ (SHELXL-97).[45] All hydrogen atoms were calculated in idealized positions with fixed displacement parameters. ORTEP-III[46] was used for the structure representation, and SCHAKAL-99[47] to illustrate molecule packing. The crystallographic data are summarized in Table 2.

X-ray Powder Diffraction. X-ray powder diffraction data were collected at a STOE StadiP X-ray powder diffractometer in transmission geometry from 5° to 30°(2Θ). Samples were placed in capillaries, and Cu Kα1 radiation was used for the measurement. Radiation was detected with a Mythen 1K detector.

Magnetic Measurements. Magnetic susceptibility data were collected using a Quantum Design MPMSR-2 or an MPMSXL-5 SQUID magnetometer under an applied field of 0.5 T over the temperature range 2−400 K in the settle mode. Samples were placed in gelatin capsules held within a plastic straw. Data were corrected for the diamagnetic contributions of the ligands by using tabulated Pascal's constants and those of the sample holder.

^{57}Fe Mössbauer Spectroscopy. Variable temperature ^{57}Fe Mössbauer measurements were recorded in transmission geometry on a constant-acceleration Wissel spectrometer loaded with a 45 mCi ^{57}Co(Rh) source from Cyclotron Ltd. The sample was sealed in a Teflon holder, and low temperature spectra were recorded using an Optistat Oxford instruments liquid nitrogen cryostat. The spectra were fitted using Recoil 1.05 Mössbauer Analysis Software.[48] The isomer shift values are given with respect to an α-Fe reference at room temperature.

Thermogravimetric Analyses. Thermogravimetric analyses were carried out on a SDT 2960 Simultaneous DSC-TGA under nitrogen atmosphere using alumina sample holder.

Differential Scanning Calorimetry. Calorimetric measurements sealed in an aluminum sample holder were carried out with a PerkinElmer DSC-7 differential scanning calorimeter at a scan rate of 10 K/min following described procedures.[49]

Table 2. Crystallographic Data of [FeL1(pina)]·2MeOH (**1**·2MeOH)

	1·2MeOH
formula	$C_{31}H_{35}FeN_5O_7$
M_r/g mol^{-1}	645.49
cryst syst	monoclinic
space group	$P2_1/c$
a/Å	13.3304(11)
b/Å	12.9564(11)
c/Å	21.5188(15)
α/deg	90
β/deg	127.769(5)
γ/deg	90
V/Å^3	2937.9(4)
Z	4
ρ/g cm^{-3}	1.459
μ/mm^{-1}	0.571
cryst size	0.32 × 0.19 × 0.11
T/K	173(2)
λ(Mo Kα)/Å	0.710 73
θ range/deg	4.19−25.38
reflns collected	11 924
indep reflns (R_{int})	5286 (0.0391)
params	391
restraints	24
$R(F)$ (all data)	0.0516 (0.0924)
wR2	0.1316
GOF	0.960

RESULTS AND DISCUSSION

Syntheses. The general synthetic pathway for the synthesis of the [FeL1(pina)] coordination polymers is given in Scheme 1. Three different synthetic modes were used to prepare the complex [FeL1(pina)](**1**) and its solvates: (i) The starting materials [FeL1($MeOH)_2$] and pina were mixed in the desired solvent and heated to reflux for 1 h, to afford **1**·0.5 MeOH, **1**·0.5 EtOH, and **1**·DMF. (ii) By slow diffusion, this method used a homemade Schlenk tube setup which was, to a given height, separated into two chambers by a dividing wall. (iii) The starting iron complex and the axial ligand were dissolved separately in the desired solvent, and the solutions were then mixed at room temperature.

The syntheses were first carried out in methanol, leading to two different samples, **1**·0.5MeOH (reflux condition, powder) and an undefined phase **1**·*x*MeOH/H_2O (diffusion setup, fine crystals). Magnetic measurements (see Magnetic Measurements section) revealed that **1**·0.5 MeOH is a pure HS complex while the sample **1**·*x*MeOH/H_2O is showing a spin transition with extremely large hysteresis around room temperature. The spin transition properties and the stability of the sample up to 400 K did raise our interest for this compound. Only a small amount of sample was obtained from the first diffusion setup, and the crystals were not of sufficient quality for single crystal X-ray structure analysis. Therefore, attempts were made to reproduce the synthesis using slow diffusion. Single crystals of sufficient X-ray quality were obtained but with a different composition (**1**·2MeOH). Magnetic measurements reveal SCO behavior with a hysteresis close to room temperature. The hysteresis loop width, however, is significantly smaller.

Since solvent has a strong influence on the SCO behavior of this system, the synthesis was repeated in different solvents: mixtures of water and methanol, ethanol, tetrahydrofuran

dx.doi.org/10.1021/ic501624b | Inorg. Chem. 2014, 53, 11563−11572

Table 3. Selected Bond Lengths [Å] and Angles [deg] of the Structure of 1·2MeOH

compound	Fe−N_{eq}	Fe−O_{eq}	Fe−N_{ax}	O_{eq}−Fe-O_{eq}	N_{ax}−Fe-N_{ax}
1·2MeOH	1.904(3)	1.940(2)	2.026(13)[a]	88.89(10)	174.4(3)[a,c]
			1.93(3)[b]		
	1.898(3)	1.947(2)	2.008(11)[a]		172.6(8)[b,c]
			2.05(3)[b]		

[a]Related to N3A. [b]Related to N3B; symmetry code. [c]1 + *x*, *y*, *z*.

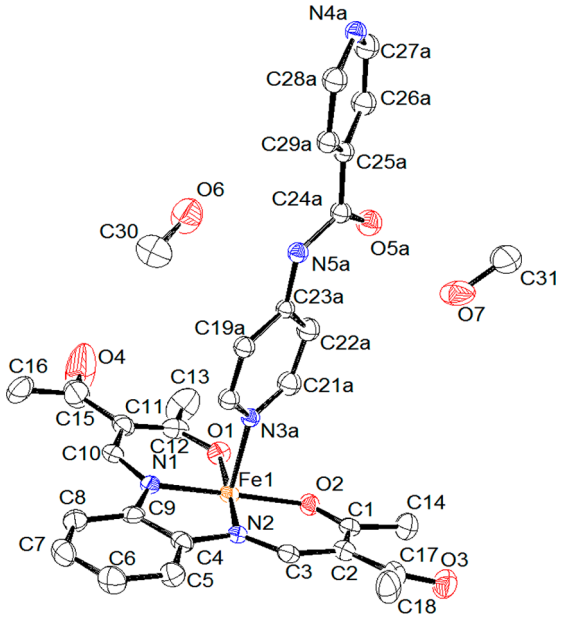

Figure 1. ORTEP drawing of the asymmetric unit of **1**·2MeOH. Hydrogen atoms and the disorder of the pina ligand have been omitted for clarity. Thermal ellipsoids are shown with a 50% probability.

(THF), and dimethylformamide (DMF). Mixtures of methanol and water were used to account for remaining water in the very hygroscopic pina ligand. This is the most likely reason for the different outcomes of the first and second diffusion setup. Indeed, in a mixture of a 98:2 ratio of methanol and water, respectively, a new powder sample **1**·0.5H_2O·0.5MeOH was obtained. Magnetic measurements of this sample show a wide hysteresis around room temperature, that is, however, not complete and unstable. Further syntheses were done with ethanol, THF, and DMF. From the synthesis in ethanol, one pure HS sample **1**·0.5EtOH was obtained, and from synthesis in THF, a further pure HS sample **1**·2H_2O. The synthesis in DMF produced an interesting phase **1**·DMF which is undergoing SCO. In Table 1, an overview of the synthesized complexes and the characteristic temperatures and $\chi_M T$ values is given. The syntheses of all samples except that of **1**·*x*MeOH/H_2O were reproduced at least once.

X-ray Structure Analysis. Crystals with the composition **1**·2MeOH were of sufficient quality for a single crystal X-ray structure analysis, and we were able to solve the structure at 173 K where the complex is in the low-spin state according to the magnetic measurements. The crystal structure of compound **1**·2MeOH describes the first example for coordination polymer with pina as axial ligand. The crystallographic data are summarized in Table 2. Selected bond lengths and angles are shown in Table 3. ORTEP drawing of the asymmetric unit is given in Figure 1.

Compound **1**·2MeOH crystallizes in the monoclinic space group $P2_1/c$. The observed bond lengths around the iron center are within the range reported for other octahedral iron(II) complexes made of this ligand type in the LS state.[7,39,50,51] The average values are 1.90 Å (Fe−N_{eq}), 1.94 Å (Fe−O_{eq}), and 2.01 Å (Fe−N_{ax}). The observed O−Fe−O angle is with 88.9° clearly indicative of LS iron(II).[7,39,50,51] The axial pina ligand links the iron centers as bridging bidentate ligand. Analysis of the polymeric structures reveals an infinite one-dimensional chain with the base vector [100]. The pina ligand is disordered, mainly concerning the asymmetric peptide bond. However, the carbonyl oxygen is pointing at the same direction in both disordered structures. This disorder could be the reason for the small steps/plateaus observed in the magnetic measurements. The asymmetric unit additionally contains two methanol molecules, each bound to the peptide bond through hydrogen bonds. The details for the hydrogen bonds are summarized in Table 4; an excerpt of the molecule packing is given in Figure 2. In one case, the hydroxy group of methanol is the donor group (O7−H7A) and the carbonyl oxygen of the peptide bond the acceptor (O5). In the other case, methanol is the acceptor (O6) of the N−H group of the peptide bond (N5−H5). This solvent molecule moreover participates in a second hydrogen bond between its hydroxy group (O6−H6A) and the carbonyl group (O3) of an adjacent equatorial ligand and, thus, is part of

Table 4. Summary of the Intermolecular Hydrogen Bonds of 1·2MeOH with d(D···A) < R(D) + R(A) + 0.5 Å, d(H···A) < R(H) + R(A) − 0.12 Å, D−H···A > 100.0°

compound	D	H	A	D−H	H···A	D···A	D−H···A
1·2MeOH	N5A	H5A	O6	0.88	2.19	3.008(6)	155
	N5B	H5B	O6	0.88	2.16	2.893(13)	141
	O7	H7A	O5A	0.84	2.09	2.887(7)	159
	O7	H7A	O5B	0.84	1.94	2.771(13)	169
	O6	H6A	O3[a]	0.84	2.04	2.865(4)	169
	C18	H18A	O7[b]	0.98	2.58	3.458(7)	149
	C18	H18C	O6[c]	0.98	2.59	3.327(5)	132
	C20A	H20A	O3[b]	0.95	2.50	3.217(10)	132

[a]Symmetry codes follow. *x*, $-^1/_2 - y$, $^1/_2 + z$. [b]$-x$, $^1/_2 + y$, $-^1/_2 - z$. [c]x, $-^1/_2 - y$, $-^1/_2 + z$.

dx.doi.org/10.1021/ic501624b | *Inorg. Chem.* 2014, 53, 11563−11572

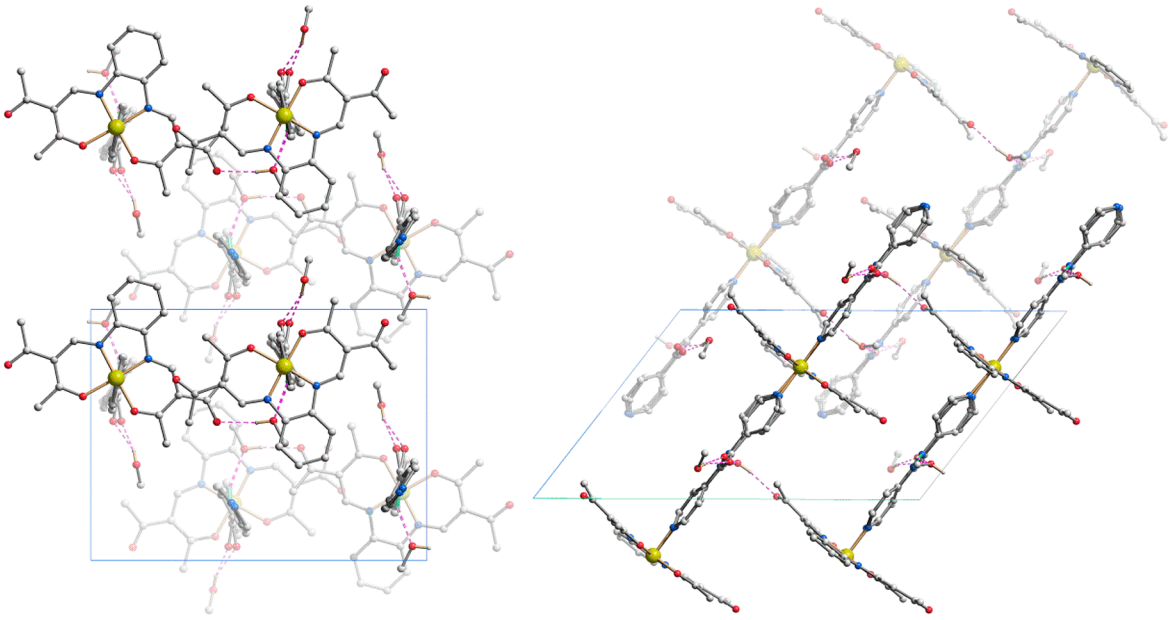

Figure 2. Crystal packing of **1**·2MeOH. View along [100] (left) and along [010] (right). Hydrogen atoms are omitted for clarity. The hydrogen bonds are given as dashed lines.

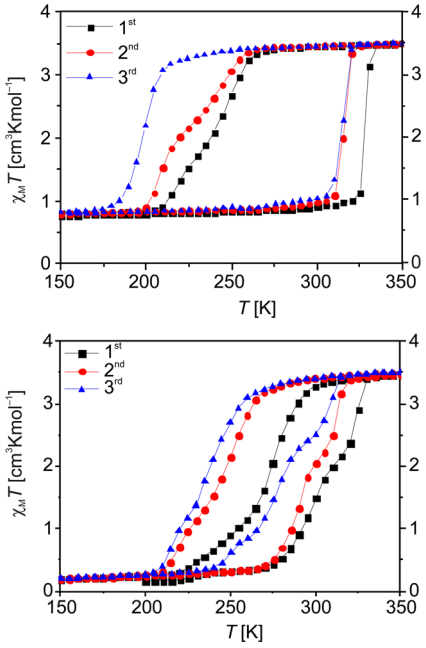

Figure 3. Plots of the $\chi_M T$ product versus T for **1**·xMeOH/H_2O (top) and **1**·2MeOH (bottom). The first loop (black squares) corresponds to measurements starting at room temperature; the sample is not heated above 350 K. Before the second loop (red circles) the sample was shortly heated to 400 K, and before the third loop (blue triangles) the sample was left at 400 K for 1 h to remove all solvent.

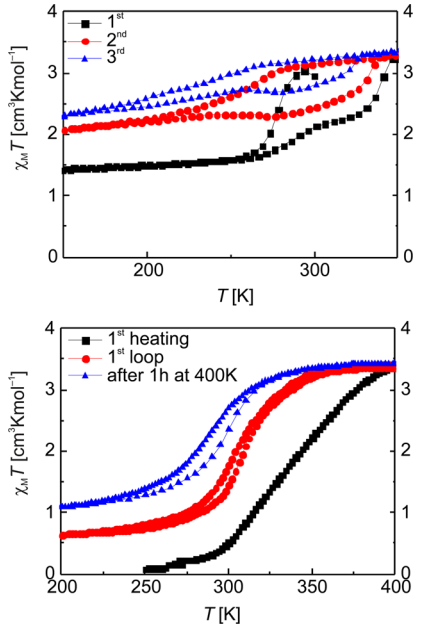

Figure 4. Plots of the $\chi_M T$ product versus T for compounds **1**·0.5H_2O·0.5MeOH (top) and **1**·DMF (bottom).

an infinite one-dimensional hydrogen bond chain (base vector [001], Figure 2). One further direct short contact is observed between the carbonyl group of the equatorial ligand and the nitrogen of the peptide bond. It should be mentioned that only the axial ligand and substituents of the equatorial ligand are involved in the hydrogen bond network and no participation of the donor oxygen atom of the equatorial ligand, as for the corresponding mononuclear imidazole complexes, is observed.

Powder X-ray Diffraction. In order to verify that the different samples of **1** assume similar structures, the calculated powder X-ray diffraction pattern of **1**·2MeOH is compared with measured PXRD patterns. The results are given in the Supporting Information, Figure S1. Indeed, in the region 2Θ = 8−8.5° and 2Θ = 26−27°, strong similarities in the diffraction patterns are observed. This can be used as confirmation that in all cases coordination polymers were formed with an approximate distance between the iron centers of 13.5 Å and a distance between the polymer chains in the region of 4 Å. The diffraction pattern of the three pure HS complexes **1**·0.5MeOH, **1**·2H_2O, and **1**·0.5EtOH are almost identical. Apparently they all precipitate in the same packing pattern independent of the

dx.doi.org/10.1021/ic501624b | Inorg. Chem. 2014, 53, 11563−11572

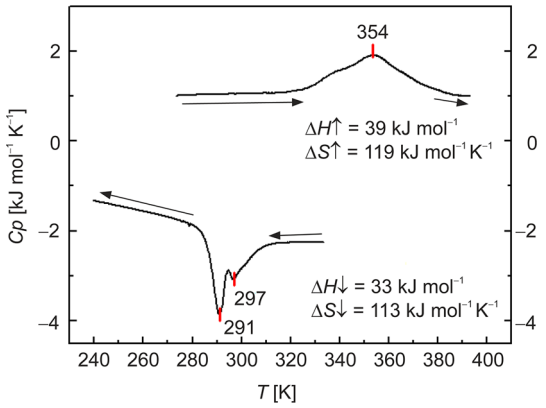

Figure 5. DSC measurement of **1**·0.5H_2O·0.5MeOH. Measured enthalpy and entropy values are given in the cooling and warming modes (5 K/min). The values were corrected by a factor 1.5 as only two-third of the iron centers are involved in the spin transition as indicated by Mössbauer spectroscopy and magnetic measurements.

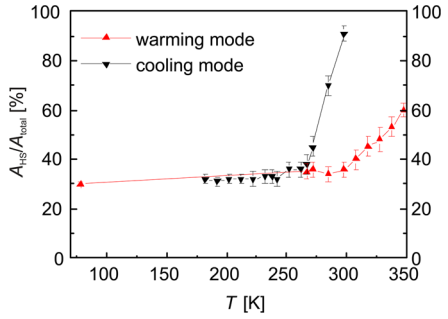

Figure 7. A_{HS}/A_{tot} [%] versus T plot of the Mössbauer spectra measured on the compound **1**·0.5H_2O·0.5MeOH.

cocrystallized solvent molecules. This assumption is supported further by the fact that the solvent-free sample of **1**·0.5MeOH (after annealing at 100 °C for 5 h under vacuum to remove all methanol) shows the same diffraction pattern as before.

The diffraction patterns of the three spin transition samples **1**·DMF, **1**·2MeOH, and **1**·0.5H_2O·0.5MeOH also show some similarities, especially in the regions 2Θ = 12−15° and 2Θ = 20−23°. There are, however, also some differences in good agreement with the different magnetic properties observed in the magnetic measurements. There are pronounced differences between the diffraction patterns of the pure HS complexes and the SCO complexes.

Magnetic Measurements. Of the seven samples investigated, three (**1**·0.5MeOH, **1**·0.5EtOH, **1**·2H_2O) are pure HS complexes in the entire temperature range with a $\chi_M T$ product in the range of 3.4 cm^3 K mol^{-1}, typical for HS iron(II). The corresponding plot of the $\chi_M T$ product versus temperature is displayed in the Supporting Information, Figure S2. For the other four samples SCO behavior is observed, which is described in the following.

The result from the magnetic measurements (plot of the $\chi_M T$ product vs T) of the undefined sample **1**·xMeOH/H_2O is displayed at the top of Figure 3. The compound shows a spin transition with a very wide thermal hysteresis around room temperature. At room temperature the $\chi_M T$ product is with 0.89 cm^3 K mol^{-1}, indicative of a sample with the majority of the spins in the LS state. Upon cooling, this value remains constant down to 50 K. Upon heating, the compound remains first in the LS state and undergoes an abrupt spin transition to the HS state above room temperature with $T_{1/2\uparrow}$ = 328 K. At

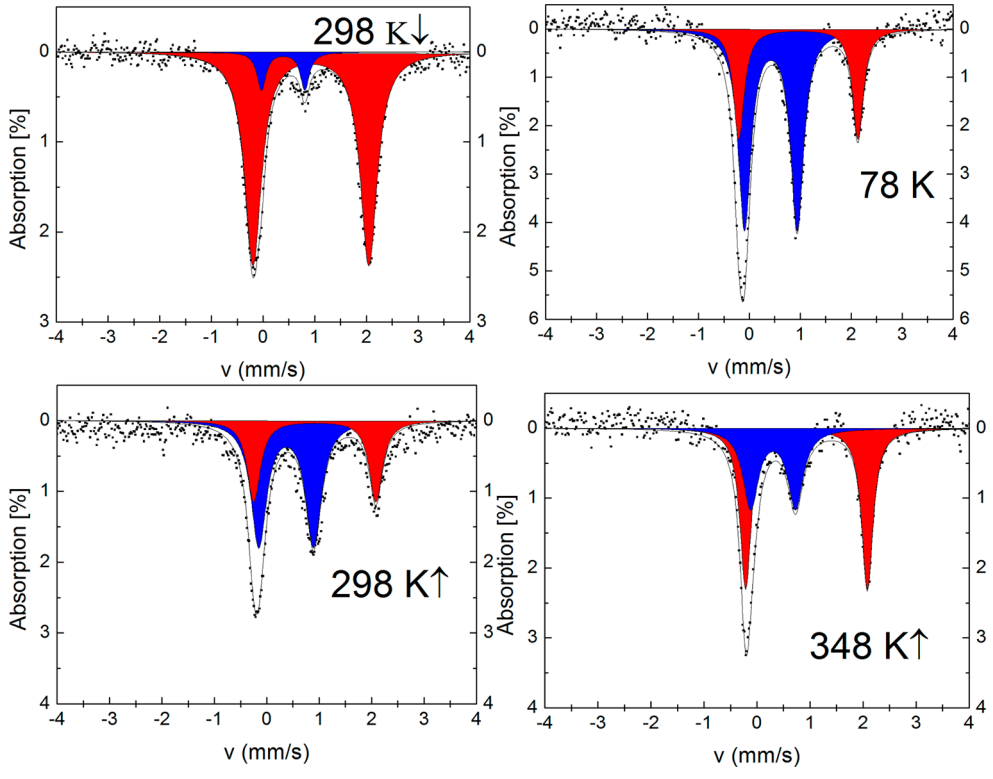

Figure 6. Selected Mössbauer spectra of **1**·0.5H_2O·0.5MeOH. HS Fe^{II} signal is depicted in red, LS Fe^{II} in blue. Measurement temperatures are indicated on the spectra.

dx.doi.org/10.1021/ic501624b | Inorg. Chem. 2014, 53, 11563−11572

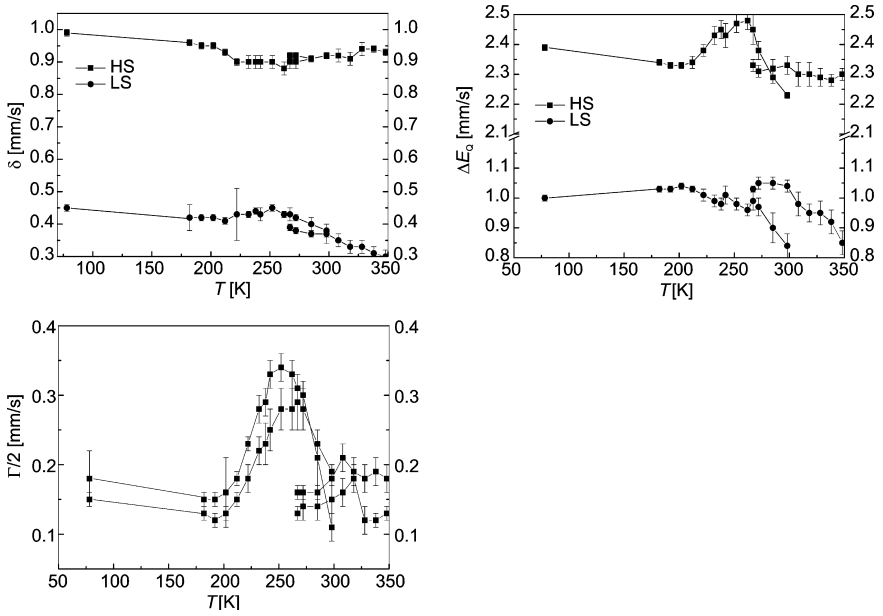

Figure 8. Plots of the isomer shift δ, quadrupole splitting ΔE_Q, and half line width $\Gamma/2$ vs T for both HS and LS signals of compound **1**·0.5 H_2O·0.5 MeOH.

350 K, the $\chi_M T$ product is with 3.49 cm^3 K mol^{-1} in the typical region for HS iron(II) complex. Upon cooling, a relatively gradual spin transition to the low-spin (LS) state is observed with $T_{1/2\downarrow}$ = 240 K and a $\chi_M T$ product of 0.79 cm^3 K mol^{-1} at 150 K. About 20% of the molecules remain in the HS state. This corresponds to an apparent thermal hysteresis of 88 K. The hysteresis is apparent in the sense that solvent molecules are released during the first warming process as first identified for [Fe(hyetrz)3](3-nitrophenylsulfonate)$_2$·3H_2O.[52] After heating to 400 K, a second loop of measurement shows that the transition temperatures are shifted to lower temperatures ($T_{1/2\downarrow}$ = 224 K and $T_{1/2\uparrow}$ = 316 K) and the hysteresis loop is with 92 K slightly wider. A closer inspection of the curve progression of the second cycle in the cooling mode reveals the formation of a slight plateau in the region of 224 K; thus, a two-step spin transition takes place while a one-step spin transition is observed during heating. The transition temperatures for the two steps are 244 and 209 K. Thus, for the second step the hysteresis width is 107 K. The difference between the first and the second cycles is most likely due to a loss of solvent molecules included in the crystal packing during the heating process. After heating the sample to 400 K for 1 h to remove all solvent, a third cycle was measured. Upon cooling, the transition temperature is again shifted to lower temperatures with $T_{1/2\downarrow}$ = 199 K, whereas, upon heating, the transition temperature remains constant ($T_{1/2\uparrow}$ = 316 K). A thermal hysteresis loop with a width of 117 K is observed! Due to difficulties with the reproduction of this sample, no further measurements on this material were possible.

Magnetic measurements of **1**·2MeOH, displayed at the bottom of Figure 3, reveal SCO behavior with a hysteresis close to room temperature. The room temperature $\chi_M T$ product of this sample is with 3.39 cm^3 K mol^{-1} in the typical region for a HS iron(II) complex. Upon heating to 350 K, it increases to a value of 3.64 cm^3 K mol^{-1}. Upon cooling, compound **1**·2MeOH undergoes a spin transition to the LS state with a $T_{1/2\downarrow}$ = 272 K and a $\chi_M T$ product of 0.2 cm^3 K mol^{-1} at 150 K. For this sample the spin transition is complete. Upon heating, the compound undergoes an abrupt spin transition back to HS state with $T_{1/2\uparrow}$ = 306 K, exhibiting a thermal hysteresis of 34 K. Indications for small steps in the heating and cooling mode are observed. The disorder of the pina ligand observed in the X-ray structure of this complex is most likely the reason for this behavior. Indeed, the pina ligand is asymmetric, having an acid-side and an amino-side, which gives the possibility for the iron centers to be coordinated twice to both ends or once to each side. This situation may result in a slight change in the crystal field strength that could be responsible for the small steps. Only the average values are considered for the following discussion. Further loops of measurement (after heating to 400 K for a few minutes and for 1 h to remove the solvent included in the material) show that the hysteresis is shifted to lower temperature once the solvent is lost. Again, this is comparable with the behavior of the first crystalline sample. The loss of the solvent is also accompanied by an increase of the hysteresis width to 51 K for the second cycle and 45 K for the third cycle.

The results of the magnetic measurements of **1**·0.5 H_2O·0.5MeOH are displayed in Figure 4. The room temperature $\chi_M T$ product is with 2.94 cm^3 K mol^{-1} indicative of an iron(II) complex that is almost completely in the HS state. Upon cooling, the compound undergoes an incomplete spin transition around 275 K, with a remaining $\chi_M T$ product of 1.41 cm^3 K mol^{-1} at 150 K (γ_{HS} = 0.4). Upon heating, the $\chi_M T$ product increases first slowly, than more rapidly, until the compound is back in the HS state in a two-step transition with an average $T_{1/2\uparrow}$ = 321 K, leading formally to a 46 K wide hysteresis. As further cycles are measured, the transition temperatures are shifted to lower temperatures, and an increase of the hysteresis width (up to 73 K for the third cycle) is observed, in agreement with the results of the previously described samples. However, for the sample **1**·0.5H_2O·0.5MeOH a significant increase of the remaining HS fraction is observed. For the third cycle, γ_{HS} = 0.65, only one-third of the iron centers undergo spin transition. In the Supporting Information, Figure S3, the TGA analysis of the sample is given to confirm the solvent loss upon heating.

dx.doi.org/10.1021/ic501624b | Inorg. Chem. 2014, 53, 11563−11572

The sample **1**·DMF (Figure 4, bottom) is at room temperature almost in the LS state. At 250 K the $\chi_M T$ product is with 0.08 cm^3 K mol^{-1} characteristic for an iron(II) LS complex. Upon heating, solvent loss accompanied by a gradual spin transition starting around 300 K and ending at 400 K is observed. The solvent loss was followed by TGA (see Experimental Section and Supporting Information, Figure S3). At 400 K in the HS state a $\chi_M T$ product of 3.35 cm^3 K mol^{-1} is obtained. The second cooling/heating cycle reveals a shift of the spin transition to lower temperatures and a small hysteresis of 4 K ($T_{1/2\downarrow}$ = 305 K, $T_{1/2\uparrow}$ = 309 K). The $\chi_M T$ product of 0.64 cm^3 K mol^{-1} at 150 K indicates that the spin state change is no longer complete but a remaining HS fraction of γ_{HS} = 0.19 is obtained. The compound was kept 1 h at 400 K in order to remove the included solvent completely. This resulted in a shift of the transition temperature to lower temperatures, an increase of the hysteresis width (10 K, $T_{1/2\downarrow}$ = 288 K, $T_{1/2\uparrow}$ = 298 K), and a higher HS fraction ($\chi_M T$ = 1.08 cm^3 K mol^{-1} at 150 K, γ_{HS} = 0.30).

All samples showing spin transition have in common that the spin transition is shifted to lower temperatures upon solvent loss and a slight increase of the hysteresis width is observed. However, for the first two samples the remaining HS fraction does not change with repeating heating/cooling cycles while for the latter two samples a significant increase for the remaining HS fraction is observed. Apparently, for the powder samples the loss of methanol, water, or DMF molecules causes the formation of defects in the crystal lattice resulting in a loss of the spin transition properties.

Mössbauer Spectroscopy and Thermal Analysis. The compound **1**·0.5H_2O·0.5MeOH was resynthesized in high amount to allow further investigations of the complex spin transition behavior using differential scanning calorimetry (DSC) and ^{57}Fe Mössbauer spectroscopy. The DSC measurements were done in order to track other phase transitions occurring upon cooling and heating that could explain the unstable ST behavior (Figure 5). Upon cooling, a first endothermic transition occurs around 297 K, which is directly followed by a sharper transition at 291 K. One transition corresponds to the incomplete HS to LS transition and the other one to another first order phase transition. Upon warming, one broad exothermic transition is observed with a maximum at 353 K corresponding to the LS to HS state spin transition, with a weak shoulder around the boiling point of methanol (≈338 K). Thus, one could assume that the loss of methanol triggers the LS to HS spin state change. Determined values of enthalpy ($\Delta H\downarrow$ = 33 kJ mol^{-1} and $\Delta H\uparrow$ = 39 kJ mol^{-1}, assuming that two-third of the iron centers switch the spin state) and entropy ($\Delta S\downarrow$ = 113 J mol^{-1} T^{-1} and $\Delta S\uparrow$ = 119 J mol^{-1} T^{-1}) are significantly higher than observed for spin transitions in similar materials[33] due to the presence of other thermodynamic phenomena occurring at the same time: another phase transition upon cooling, and the methanol vaporization upon heating. Obviously, those phenomena are related to the spin transitions. The small difference of transition temperatures when one compares the DSC results to the SQUID measurement originates from the different measurements modes (sweep for the DSC, settle for the SQUID).

^{57}Fe Mössbauer spectrometry was used to understand the incompleteness of the spin transition of the powder phase **1**·0.5H_2O·0.5MeOH. Mössbauer parameters of all spectra are summarized in the Supporting Information, Table S1. Selected spectra are shown in Figure 6. A plot of the A_{HS}/A_{tot} versus T is shown in Figure 7, assuming equal Debye−Waller factors for the LS and HS ions. The spectrum at 298 K shows two different signals: one quadrupole doublet corresponding to HS iron(II) ions with a large quadrupole splitting (δ = 0.92(1) mm/s; ΔE_Q = 2.24(1) mm/s; $\Gamma/2$ = 0.20(2) mm/s; A_{HS}/A_{tot} 93(3)%) and another quadrupole doublet corresponding to LS iron(II) ions with a smaller quadrupole splitting (δ = 0.38(2) mm/s; ΔE_Q = 0.84(4) mm/s; $\Gamma/2$ = 0.11(2) mm/s; A_{LS}/A_{tot} 7(3)%). The hyperfine parameters are similar to reported ones for 1D chains of complexes with similar ligand system.[53] In the following, the Mössbauer spectra were first recorded upon cooling down to 78 K, then upon warming up to 348 K. Upon cooling, the compound undergoes an incomplete spin transition with a $T_{1/2\downarrow}$ = 280 K, with a remaining HS area of 30% at 78 K. The transition temperature is in good agreement with the results from the magnetic measurements (275 K); however, the spin transition is more complete. This can be explained because the Mössbauer measurements are done in closed Teflon capsules at ambient pressure. In contrast to this in the SQUID magnetometer the sample is in constant vacuum. The results of the SQUID measurements on this sample show that upon solvent loss the spin transition is less complete. Upon warming, the HS fraction remains constant up to 298 K. Above 298 K, the LS to HS conversion starts, that is, however, not complete at 348 K.

The spectrum at 298 K after the first cooling shows a different population of the two iron(II) states compared to the first spectrum at 298 K. Thus, clear evidence for the room temperature bistability is obtained. The sample was further heated up to 348 K, showing an increase of the HS fraction at higher temperatures. The analysis of isomer shift δ, quadrupole splitting ΔE_Q, and half line width $\Gamma/2$ with respect to the temperature reveals that all parameters show some modifications upon cooling between 272 and 232 K. Especially, the line width suddenly raises to high values (at 252 K, $\Gamma/2$ = 0.28(3) mm/s for the HS state and 0.34(3) mm/s for the LS state). The plots of the Mössbauer parameters versus T are shown in Figure 8. This sudden jump, which is occurring right after the spin transition around 250 K upon cooling, is attributed to a phase transition. This is in good agreement with the results from the DSC measurements that a phase transition is occurring during the HS to LS spin transition. Mössbauer spectroscopy therefore allows attributing the DSC peak at 297 K (Figure 5) to the spin transition and the sharper peak at 291 K to the phase transition. However, the exact nature of the phase transition (changes in the hydrogen bond network, reorientation of the ligand) is yet to be determined. The results support the tendency that wide hysteresis loops are observed, when the spin transition is accompanied by pronounced structural changes.[35]

One further piece of important information from Mössbauer spectroscopy is that only one iron site is observed for the HS and the LS state. This implies that the coordination spheres of the iron centers are not changed after the phase transition or the loss of solvent. Therefore, the phase transition could be a rearrangement of the hydrogen bond network, as it was already discussed for similar systems.[12] Another possibility would be changes in the orientation of the ligand, e.g., the rotation of the axial ligand from eclipsed to staggered.

For compound **1**·0.5H_2O·0.5MeOH, the unstable character of the SCO is most likely due to the loss of methanol during the LS to HS spin transition. On the basis of the powder diffraction pattern of **1**·0.5H_2O·0.5MeOH (partially dried

sample) it is difficult so say if the solvent-free sample is identical to the annealed sample **1** obtained from the pure HS complexes or if another pure HS phase is obtained.

CONCLUSION

We hereby reported the synthesis of seven solvates of the coordination polymer [FeL1(pina)] (**1**) showing either spin crossover or being HS depending on the type of solvent used. Compound **1**·xH$_2$O/MeOH, obtained as crystals, shows a very wide hysteresis of 88 K. Attempts to repeat the synthesis of those crystals led to new compound **1**·2MeOH, presenting a wide hysteresis of up to 51 K around room temperature. The crystal structure of **1**·2MeOH was determined, showing 1D coordination polymers linked together by an hydrogen bond network, therefore creating a 2D network through the crystal packing. Thus, the pina ligand was used successfully in a crystal-engineering-like approach to improve the spin transition properties of the iron(II) coordination polymers with regard to the observation of thermal hysteresis loops. The thermal hystereses are wider than those observed for related complexes with rigid ligands as 4,4′-bipyridine[54] or with modified equatorial ligands.[37] From other methods of synthesis, the compound **1**·0.5H$_2$O·0.5MeOH was obtained. This latter sample shows also a wide hysteresis loop of 46 K around room temperature. However, this compound is not stable upon heating, being turned into an HS compound **1**·xH$_2$O upon loss of methanol. The compound **1**·0.5H$_2$O·0.5MeOH was analyzed with DSC and Mössbauer spectrometry. Finally, the compound **1**·DMF was obtained from synthesis in DMF. This latter compound shows a gradual spin crossover, but once the solvent is removed under vacuum, it shows a hysteresis of 10 K around room temperature. All the reported compounds show that their spin crossover properties strongly depend on the included solvent molecules and are most likely driven by the intermolecular interactions through a hydrogen bond network, as expected by choosing the pina ligand for synthesis of coordination polymers. This work confirms our concept that hydrogen bonds have the optimal balance between elasticity and rigidity to communicate the structural changes upon spin transition from one molecule to another. With the concept of Halcrow,[35] pronounced structural changes are necessary for the observation of ferroelastic properties (hysteresis[55]) in spin crossover materials. The combination of equatorial and axial ligands might be especially suited to allow such changes. Next to changes in the hydrogen bond network, e.g., a rotation of the axial ligand is possible. Further work is ongoing in the synthesis of derivatives of the pina ligand in order to form even stronger hydrogen bond networks.

ASSOCIATED CONTENT

Supporting Information

Summary of Mössbauer parameters of all spectra in Table S1, PXRD pattern of the different samples in Figure S1, plot of the $\chi_M T$ product vs T of **1**·0.5MeOH, **1**·0.5EtOH, **1**·2H$_2$O in Figure S2, and TGA results of **1**·0.5H$_2$O·0.5MeOH and **1**·DMF in Figure S3. This material is available free of charge via the Internet at http://pubs.acs.org.

AUTHOR INFORMATION

Corresponding Authors

*E-mail: yann.garcia@uclouvain.be.
*E-mail: weber@uni-bayreuth.de.

Author Contributions

The manuscript was written through contributions of all authors. All authors have given approval to the final version of the manuscript.

Notes

The authors declare no competing financial interest.

ACKNOWLEDGMENTS

We thank Florian Puchtler (University of Bayreuth) for the collection of powder diffraction data. Further, we thank the Fonds National de la Recherche Scientifique-FNRS and the COST action CM1305, as well as GFSM for allowing C.L. and A.P.R. to attend GFSM 2012. Support from the University of Bayreuth, the Deutsche Forschungsgemeinschaft (WE 3546_4-1 and SFB 840/A10), and the Fonds der Chemischen Industrie is gratefully acknowledged.

REFERENCES

(1) *Spin-Crossover Materials*; Halcrow, M. A., Ed.; John Wiley & Sons Ltd.: Chichester, U.K., 2013.
(2) *Spin Crossover in Transition Metal Compounds I–III*; Gütlich, P., Goodwin, H., Eds.; Springer: Berlin, 2004.
(3) Gütlich, P.; Hauser, A.; Spiering, H. *Angew. Chem., Int. Ed.* **1994**, *33*, 2024–2054.
(4) Letard, J.-F. *J. Mater. Chem.* **2006**, *16*, 2550–2559.
(5) Sato, O.; Tao, J.; Zhang, Y.-Z. *Angew. Chem., Int. Ed.* **2007**, *46*, 2152–2187.
(6) Kitchen, J. A.; Brooker, S. *Coord. Chem. Rev.* **2008**, *252*, 2072–2092.
(7) Weber, B. *Coord. Chem. Rev.* **2009**, *253*, 2432–2449.
(8) Halcrow, M. A. *Coord. Chem. Rev.* **2009**, *253*, 2493–2514.
(9) Murray, K. S. *Aust. J. Chem.* **2009**, *62*, 1081–1101.
(10) Gaspar, A.; Seredyuk, M.; Gütlich, P. *J. Mol. Struct.* **2009**, *924–926*, 9–19.
(11) Brooker, S.; Kitchen, J. A. *Dalton Trans.* **2009**, 7331–7340.
(12) Koudriavtsev, A. B.; Linert, W. *J. Struct. Chem.* **2010**, *51*, 335–365.
(13) Real, J. A.; Gaspar, A. B.; Munoz, M. C. *Dalton Trans.* **2005**, 2062–2079.
(14) Klingele, J.; Kaase, D.; Schmucker, M.; Lan, Y.; Chastanet, G.; Létard, J.-F. *Inorg. Chem.* **2013**, *52*, 6000–6010.
(15) Petzold, H.; Heider, S. *Eur. J. Inorg. Chem.* **2011**, *2011*, 1249–1254.
(16) Khusniyarov, M. M.; Weyhermüller, T.; Bill, E.; Wieghardt, K. *Angew. Chem., Int. Ed.* **2008**, *47*, 1228–1231.
(17) Stock, P.; Pędziński, T.; Spintig, N.; Grohmann, A.; Hörner, G. *Chem.—Eur. J.* **2013**, *19*, 839–842.
(18) Cambi, L.; Szegö, L. *Ber. dtsch. Chem. Ges. A/B* **1933**, *66*, 656–661.
(19) Cambi, L.; Szegö, L. *Ber. dtsch. Chem. Ges. A/B* **1931**, *64*, 2591–2598.
(20) Kahn, O. *Science* **1998**, *279*, 44–48.
(21) Létard, J.-F.; Guionneau, P.; Goux-Capes, L. *Spin Crossover in Transition Metal Compounds I–III*; Gütlich, P., Goodwin, H., Eds.; Springer: Berlin, 2004; pp 221–249.
(22) Galet, A.; Gaspar, A. B.; Muñoz, M. C.; Bukin, G. V.; Levchenko, G.; Real, J. A. *Adv. Mater.* **2005**, *17*, 2949–2953.
(23) Linares, J.; Codjovi, E.; Garcia, Y. *Sensors* **2012**, *12*, 4479–4492.
(24) Coronado, E.; Galán-Mascarós, J. R.; Monrabal-Capilla, M.; García-Martínez, J.; Pardo-Ibáñez, P. *Adv. Mater.* **2007**, *19*, 1359–1361.
(25) Forestier, T.; Mornet, S.; Daro, N.; Nishihara, T.; Mouri, S.-i.; Tanaka, K.; Fouche, O.; Freysz, E.; Letard, J.-F. *Chem. Commun.* **2008**, 4327–4329.
(26) Göbel, C.; Palamarciuc, T.; Lochenie, C.; Weber, B. *Chem.—Asian J.* **2014**, *9*, 2232–2238.

(27) Kuroiwa, K.; Kikuchi, H.; Kimizuka, N. *Chem. Commun.* **2010**, *46*, 1229−1231.
(28) Seredyuk, M.; Gaspar, A. B.; Ksenofontov, V.; Galyametdinov, Y.; Verdaguer, M.; Villain, F.; Gütlich, P. *Inorg. Chem.* **2008**, *47*, 10232−10245.
(29) Carmen Muñoz, M.; Antonio Real, J. *Spin-Crossover Materials*; Halcrow, M. A., Ed.; John Wiley & Sons Ltd.: New York, 2013; pp 121−146.
(30) Roubeau, O. *Chem.—Eur. J.* **2012**, *18*, 15230−15244.
(31) Schlamp, S.; Thoma, P.; Weber, B. *Chem.—Eur. J.* **2014**, *20*, 6462−6473.
(32) Weber, B.; Bauer, W.; Obel, J. *Angew. Chem., Int. Ed.* **2008**, *47*, 10098−10101.
(33) Weber, B.; Bauer, W.; Pfaffeneder, T.; Dîrtu, M. M.; Naik, A. D.; Rotaru, A.; Garcia, Y. *Eur. J. Inorg. Chem.* **2011**, *2011*, 3193−3206.
(34) Schlamp, S.; Weber, B.; Naik, A. D.; Garcia, Y. *Chem. Commun.* **2011**, *47*, 7152−7154.
(35) Halcrow, M. A. *Chem. Soc. Rev.* **2011**, *40*, 4119−4142.
(36) Weber, B.; Obel, J.; Henner-Vasquez, D.; Bauer, W. *Eur. J. Inorg. Chem.* **2009**, *2009*, 5527−5534.
(37) Bauer, W.; Lochenie, C.; Weber, B. *Dalton Trans.* **2014**, *43*, 1990−1999.
(38) Kumar, D. K.; Jose, D. A.; Dastidar, P.; Das, A. *Langmuir* **2004**, *20*, 10413−10418.
(39) (a) Nowak, R.; Bauer, W.; Ossiander, T.; Weber, B. *Eur. J. Inorg. Chem.* **2013**, *2013*, 975−983. (b) Costa, J. S.; Rodríguez-Jiménez, S.; Craig, G. A.; Barth, B.; Beavers, C. M.; Teat, S. J.; Aromí, G. *J. Am. Chem. Soc.* **2014**, *136*, 3869−3874. (c) Gómez, V.; Benet-Buchholz, J.; Martin, E.; Galán-Mascarós, J. R. *Chem.—Eur. J.* **2014**, *20*, 5369−5379.
(40) Becker, H. G. O. Organikum. *Organisch-Chemisches Grundpraktikum*, 19th ed.; Johann Ambrosius Barth: Berlin, 1993.
(41) Wolf, L.; Jäger, E.-G. *Z. Anorg. Allg. Chem.* **1966**, *346*, 76−91.
(42) Weber, B.; Betz, R.; Bauer, W.; Schlamp, S. *Z. Anorg. Allg. Chem.* **2011**, *637*, 102−107.
(43) Jäger, E.-G.; Häussler, E.; Rudolph, M.; Schneider, A. *Z. Anorg. Allg. Chem.* **1985**, *525*, 67−85.
(44) Altomare, A.; Burla, M. C.; Camalli, M.; Cascarano, G. L.; Giacovazzo, C.; Guagliardi, A.; Moliterni, A. G. G.; Polidori, G.; Spagna, R. *J. Appl. Crystallogr.* **1999**, *32*, 115−119.
(45) Sheldrick, G. *Acta Crystallogr., Sect. A* **2008**, *64*, 112−122.
(46) Farrugia, L. *J. Appl. Crystallogr.* **1997**, *30*, 565.
(47) Keller, E. *Schakal-99*; University of Freiburg: Freiburg, Germany, 1999.
(48) Lagarec, K.; Rancourt, D. G. *Recoil, Mössbauer Spectral Analysis Software for Windows 1.0*; Department of Physics, University of Ottawa: Canada, 1998.
(49) Rotaru, A.; Dîrtu, M. M.; Enachescu, C.; Tanasa, R.; Linares, J.; Stancu, A.; Garcia, Y. *Polyhedron* **2009**, *28*, 2531−2536.
(50) Bauer, W.; Scherer, W.; Altmannshofer, S.; Weber, B. *Eur. J. Inorg. Chem.* **2011**, 2803−2818.
(51) Pfaffeneder, T. M.; Thallmair, S.; Bauer, W.; Weber, B. *New J. Chem.* **2011**, *35*, 691−700.
(52) Garcia, Y.; van Koningsbruggen, P. J.; Codjovi, E.; Lapouyade, R.; Kahn, O.; Rabardel, L. *J. Mater. Chem.* **1997**, *7*, 857−858.
(53) Bauer, W.; Pfaffeneder, T.; Achterhold, K.; Weber, B. *Eur. J. Inorg. Chem.* **2011**, 3183−3192.
(54) Weber, B.; Tandon, R.; Himsl, D. *Z. Anorg. Allg. Chem.* **2007**, *633*, 1159−1162.
(55) Salje, E. K. *Annu. Rev. Mater. Res.* **2012**, *42*, 265−283.